RevMexAA (Serie de Conferencias), **1**, 77-84 (1995)

THE NATURE OF THE RADIO SOURCES WITHIN CEPHEUS A EAST

Guido Garay
Departamento de Astronomía, Universidad de Chile
Casilla 36-D, Santiago, Chile

RESUMEN

La fuente de radio Cefeo A-Este consta de 16 componentes compactas ($\sim 1''$), situadas dentro de una región de $25''$ de radio, la mayoría de las cuales se encuentran en estructuras alargadas ubicadas en los bordes de fragmentos moleculares densos. En esta contribución se resumen los resultados de observaciones en el continuo de radio, usando el VLA en varias frecuencias y con haces similares, realizadas con el propósito de determinar los índices espectrales de las múltiples componentes de dicha región. Encontramos que los índices espectrales de la emisión de radio de las fuentes compactas, en el intervalo de frecuencia entre 1.5 y 15 GHz, cubre un amplio rango que va desde −0.6 a 0.7. Los objetos 2 y 3d, las fuentes de radio más brillantes dentro de Cefeo A-Este, presentan morfologías alargadas y dependencias del tamaño angular y de la densidad de flujo con la frecuencia, indicando que corresponden a chorros de gas ionizado. Sugerimos que estos dos objetos son responsables de gran parte de los fenómenos de flujo y excitación observados en esta región. Los objetos que forman las cuerdas exhiben, a través de su extensión, una mezcla de índices espectrales planos y negativos, indicando la presencia de emisión tanto térmica como no térmica. Sugerimos que la emisión de radio, proveniente de las cuerdas, surge de choques que resultan de la interacción de vientos estelares colimados con el medio ambiente.

ABSTRACT

The Cepheus A-East radio source is known to consist of 16 compact ($\sim 1''$) components, clustered within a $25''$ radius region, most of which are aligned in string-like structures located at the edge of dense molecular clumps. In this contribution we summarize the results of multi-frequency, matching beam, radio continuum observations of the Cep A-East region made with the VLA, which were designed to determine the spectral indices of the radio emission from its multiple components. We find that the spectral indices of the integrated emission from the compact objects, in the frequency interval from 1.5 to 15 GHz, cover a wide range, from −0.6 to 0.7. Objects 2 and 3d, the brightest sources within Cep A-East, show elongated morphologies and angular size and flux density dependences with frequency which indicate they correspond to confined jets of ionized gas. We suggest that these two objects are responsible for most of the complex outflow and excitation phenomena observed in the region. The objects appearing in string structures exhibit a mixture of flat and negative spectral indices across their faces, indicating the presence of both thermal and non-thermal emission. We suggest that the radio emission from the string sources arises in shocks resulting from the interaction of confined stellar winds with the surrounding medium. The duality in emission mechanisms is expected in shock waves where a small fraction of the electrons are accelerated to relativistic velocities, giving rise to non-thermal emission, while most of the electrons produce thermal free-free emission.

Key words: **ISM: H II REGIONS — ISM: JETS AND OUTFLOWS — RADIO CONTINUUM: STARS — STARS: FORMATION**

1. INTRODUCTION

Cepheus A, located at the distance of 725 pc, is the densest condensation within the Cepheus OB3 molecular cloud complex (Sargent 1977). It is known to be an active region of star formation, as indicated by the presence of H_2O masers (Blitz & Lada 1979; Lada et al. 1981; Cohen, Rowland, & Blair 1984), OH masers (Rodríguez et al. 1980; Cohen et al. 1984), Herbig-Haro objects (Hartigan & Lada 1985; Hartigan et al. 1986; Lenzen 1988; Corcoran, Ray, & Mundt 1993), and infrared sources (Lenzen 1988). In addition it contains powerful mass outflows. Rodríguez , Ho, & Moran (1980) first reported a high velocity bipolar molecular outflow, oriented roughly in an east-west direction and centered on Cep A-East. Further observations, with higher sensitivity and angular resolution, revealed a more complex morphology for the outflow, including multiple lobes of emission (Hayashi, Hasegawa, & Kaifu 1988, Bally & Lane 1991). The driving source (or sources) of the molecular outflows have been difficult to determine. The bolometric luminosity of the whole region is about $2.5 \times 10^4\ L_\odot$ (Evans et al. 1981).

Two main regions of ionized gas, separated by $\sim 1\farcm5$, have been detected toward Cepheus A: Cep A-East and Cep A-West (Hughes & Wouterloot 1982; Rodríguez & Cantó 1983). It is upon the first region that I will concentrate on this paper. A wealth of VLA radio continuum observations, made over the course of the last decade, have shown that Cep A-East consist of several compact sources, most of them appearing in string-like structures (Hughes & Wouterloot 1984, Hughes 1985, 1988, 1991). A total of sixteen compact ($\sim 1''$) components, clustered within a region of $\sim 25''$ in radius centered near the H_2O maser activity, have been identified. In spite of the numerous studies, a clear understanding of the mechanism of emission and the nature of the compact radio sources within Cep A-East did not emerged. Hughes & Wouterloot (1984) and Hughes (1985) suggested that about a dozen of the objects represent very young, $\sim 10^3$ years old, H II regions each of them excited by a B3 star. This interpretation has, however, been questioned on several grounds (cf. Torrelles et al. 1986). For instance, it is difficult to explain how all stars could be at about the same stage of evolution or why they were formed in lines.

2. OBSERVED CHARACTERISTICS OF THE RADIO EMISSION

In this contribution we summarize the results of multiwavelength radio continuum observations, made with the VLA, of the Cep A-East region which were designed to determine the spectral indices of the radio emission from their multiple components. A detailed discussion of the observed characteristics of these sources and of their physical nature is presented elsewhere (Rodríguez et al. 1994; Garay et al. 1995). The knowledge of the spectral indices have helped to establish the nature of the radio emission and to determine which of the compact radio objects are internally excited, allowing in turn to identify the powering sources of the activity within the Cep A-East region. Figure 1 shows a map of the radio emission from Cep A-East, at the wavelength of 20 cm, with angular resolution of $1\farcs2$. Sources are designated with the numbers and letters given by Hughes & Wouterloot (1984).

2.1. Morphologies

The string features (see Fig. 1) appear as elongated structures of diffuse and weak emission with typical lengths of $\sim 15''$ ($\sim$0.05 pc at the distance of 725 pc) containing chains of relatively brighter compact cores. The individual components of the strings (sources 1a, 1b, 4, 5, 6, 7a, 7b, and 7c) are characterized by exhibiting irregular, clumpy morphologies. On the other hand, the radio sources located at the center of the Cep A-East region (objects 2, 3b, 3c, and 3d) are characterized by being brighter and more compact than the string sources.

2.2. Spectral Indices

The radio emission from the compact objects within Cep A-East span a wide range in spectral indices, from -0.6 to 1.0. This is clearly appreciated in Figure 2 **(Plate 2)**, which shows an image of the spectral index α, where α is defined by $S_\nu \propto \nu^\alpha$, S_ν is the flux density and ν is the frequency, between 20 and 2 cm. This remarkable image reveals that across objects 1a, 5, 7b, and 7c a range of spectral indices are seen, from -0.6 to 0.0, indicating a mixture of thermal and non-thermal emission. Sources 1b, 4, 6, and 7a exhibit spectral indices in the range $-0.3 \leq \alpha \leq 0.1$, consistent, within the errors, with the value expected for optically thin free-free emission of -0.1. The spectral indices toward sources 2, 3b, 3c, and 3d are positive ($\alpha \geq 0.3$), with object 2 exhibiting the highest value. The spectral indices of the integrated flux density from each object, which includes

the emission from both the brighter cores and from the diffuse envelopes, range from −0.6 to 0.7 (see Table 1). Sources 1a, 5, 7b, and 7c exhibit considerably negative indices ($\alpha \leq -0.4$), those of sources 1b, 4, 6, and 7a are in the range from −0.3 to −0.1. The integrated flux density versus frequency of selected radio sources within the Cep A-East region are shown in Figure 3. The continuous line corresponds to the result of a least squares fit to the observed spectrum. We note that the spectral indices of the emission from the diffuse envelopes of the string sources are slightly different (usually more negative) than those of the emission from their more compact cores.

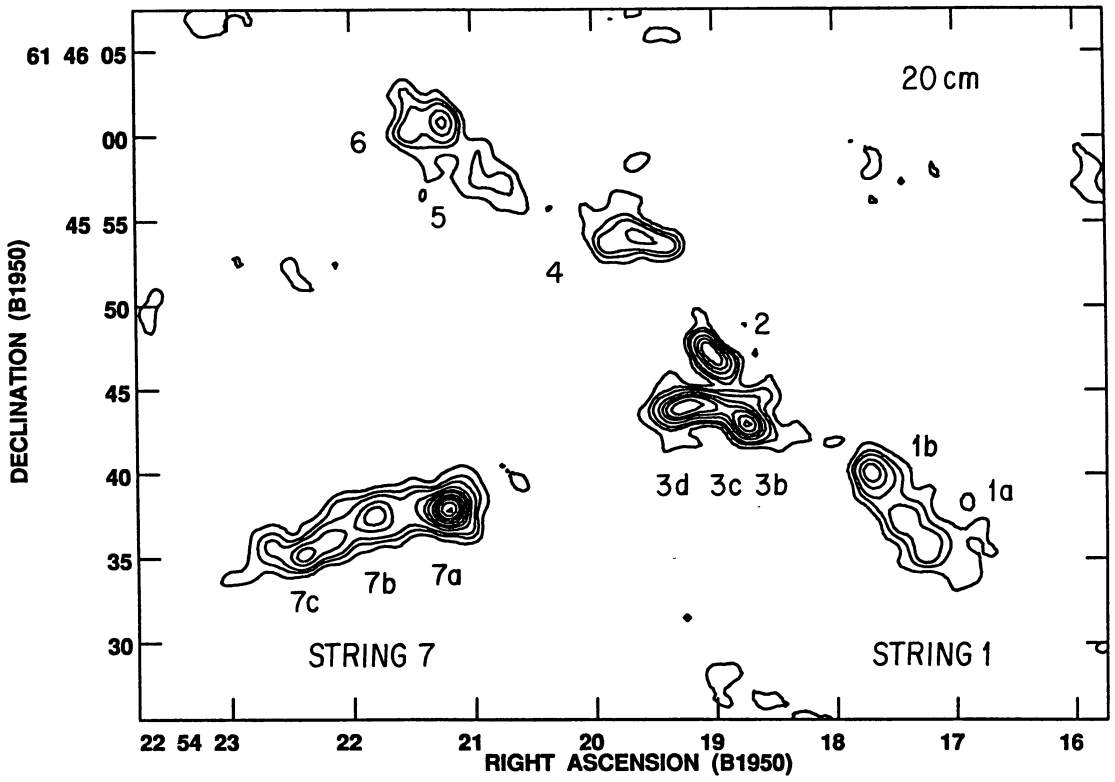

Fig. 1.— VLA radio continuum map of the Cep A-East region, at 20 cm with 1.″2 angular resolution. Contour levels are −1, 1, 2, 3, 5, 7, 9, 12, 15, 18, 22, and 26 times 0.15 mJy per beam.

3. NATURE OF THE RADIO SOURCES

Based on many different lines of evidence we have classified the radio objects within the Cep A-East region in two main groups: internally excited and externally excited objects. In this section we summarize the physical nature of most of the objects.

3.1. Objects which Harbour Energy Sources

Objects 2, 3a, 3c, 3d, 8, and 9 are likely to have an energy source of their own, as indicated by their association to H_2O and OH masers condensations (objects 2, 3a, and 3d; Lada et al. 1981; Cohen et al. 1984), variability in their flux density (objects 3a, 8, and 9), positive spectral indices (objects 2, 3c, and 3d), and association to infrared point sources (object 3a; Lenzen 1988). Even though these sources share similar characteristics in the radio band, such as being the most compact and brighter within the Cep A-East region, they appear to have different physical characteristics.

Table 1. Spectral indices

Source	Position		Sp. index
	$\alpha(1950)$	$\delta(1950)$	
1a.....	$22^h54^m17^s.27$	$61°45'35''.7$	−0.59
1b.....	17.68	40.0	−0.27
2.....	19.04	47.3	0.67
3b.....	18.74	42.9	−0.01
3c.....	19.02	43.9	0.39
3d.....	19.26	43.9	0.28
4.....	19.56	53.9	−0.22
5.....	20.77	57.4	−0.51
6.....	21.25	46 0.8	−0.28
7a.....	21.22	45 37.7	−0.14
7b.....	21.81	37.4	−0.37
7c.....	22.42	35.2	−0.39

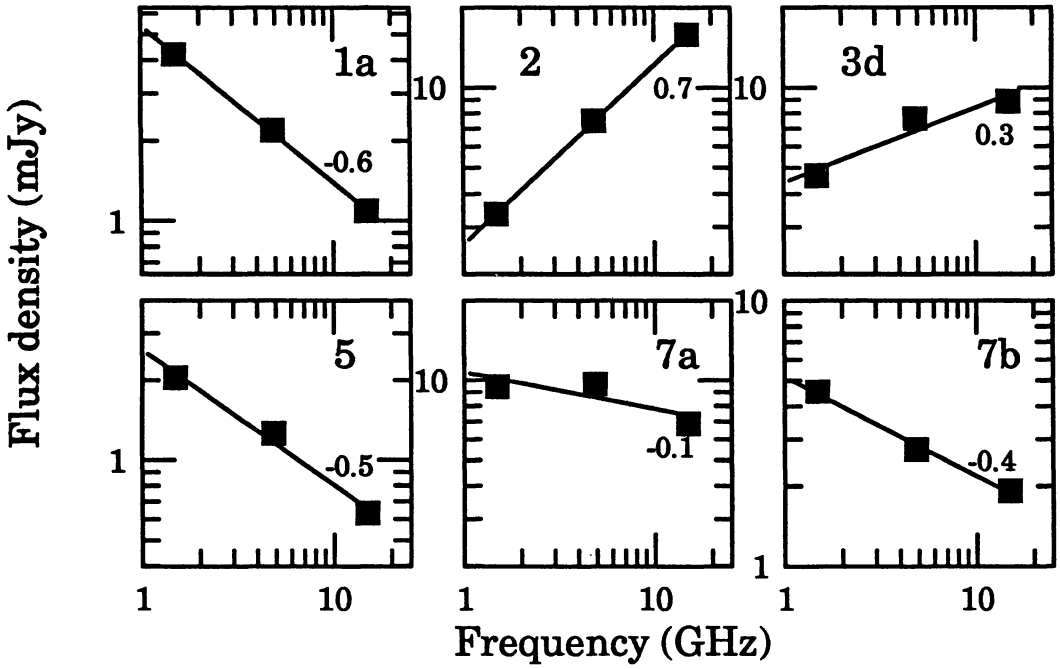

Fig. 3.— Radio continuum flux density versus frequency for selected sources within the Cep A-East region. In each panel the continuous line represents a minimum least squares power law fit to the observed spectra of the object indicated at the top. Also given is the fitted power law index.

3.1.1. Thermal Jets: Objects 2 and 3d

Object 2, the brightest radio source at 15 GHz, is believed to be associated with the most luminous source in the region. Our observations show that this object is elongated in the direction at a P.A. of 44°±4° and that is unresolved in the orthogonal direction, having and opening angle of ∼15°. Further, the angular size of

the major axis decreases with frequency as $\nu^{-0.6}$. We also find that the total flux density, in the 1.5 to 43.3 GHz range, is well fitted by a power law of the form $\nu^{0.7}$. These dependences can be well explained by a model in which the emission is thermal emission arising from a confined thermal jet of ionized gas. For a collimated wind of constant temperature, velocity, and ionization fraction, the flux density and angular size of the source depend on frequency as $S_\nu \propto \nu^{1.3-0.7/\epsilon}$ and $\theta_\nu \propto \nu^{-0.7/\epsilon}$, respectively, where ϵ is the power law index that describes the dependence of the jet half-width, w, (perpendicular to the jet axis) with the distance to the jet origin (Reynolds 1986). Within observational error, object 2 can be interpreted as a purely biconical (ϵ=1) jet. In addition, we find that the spectral index of the emission from source 2 is not constant along its major axis, but decreases toward the edges, a result consistent with a model in which the thermal jet is resolved (Reynolds 1986).

Using the observed flux density and opening angle, assuming an electron temperature of 10^4 K, $\epsilon = 1$, and that the jet axis is nearly perpendicular to the line of sight, we find that (see eqn.[19] of Reynolds 1986) $\dot{M}_w\ v_w^{-1}$=1.1 $\times 10^{-3}$ $M_\odot$ yr^{-1} km^{-1} s, where $\dot{M}_w$ and v_w are, respectively, the ionized mass loss-rate and the velocity of the biconical stellar wind. Further, assuming that the radio emission from the strings components with flat spectrum located in the direction of the jet is free-free emission from a shocked wind (see §3.2) gives a second condition between the mass loss rate and velocity of the stellar wind, from which we derive that the jet stellar wind from source 2 has a mass loss rate of 2×10^{-6} $M_\odot$ yr^{-1} and a velocity of 1900 km s^{-1} (Garay et al. 1995). The momentum rate injected by the jet into the surrounding medium is $\sim 4\times10^{-3}$ $M_\odot$ yr^{-1} km s^{-1} , value consistent with the lower limit for the momentum rate of the molecular outflow derived by Rodríguez et al. (1982). Then, it appears possible that the jet could be driving the outflow in the frame of the unified stellar jet/molecular outflow model of Raga et al. (1993).

Object 3d is elongated in a direction at a P.A. of 107°±4° and unresolved in the orthogonal direction. At 15 GHz we measured an elongation ratio of $\sim$ 9, implying an opening angle (for a jet like geometry) equal to or smaller than 13°. The angular size of the major axis decreases with increasing frequency as $\nu^{-0.3}$. In addition, the flux density increases with frequency as $\nu^{0.3}$. These results suggest that the radio emission from object 3d also arises from a collimated ionized wind. The power law dependences with frequency of the angular size and flux density are similar to those derived for the exciting source of the HH 80-81 system of Herbig-Haro objects (Martí, Rodríguez , & Reipurth 1993). The observed dependences appear to depart significantly from the purely biconical case and can not be explained by a simple jet model with constant temperature, velocity, and ionization fraction. They may be possible explained assuming that one or more of these parameters varies with the distance from the jet center (Reynolds 1986).

Observations at 15 GHz with angular resolution of $\sim$ 0.″1, carried out with the VLA by Hughes (1988), show that the cores of objects 2 and 3d consist of two ultracompact components ($\leq$ 0.″1 in size) separated by $\sim$ 0.″2. The lines joining the two ultracompact sources within objects 2 and 3d are, respectively, at P.A. of ~40° and 114°, namely roughly in the same directions as that of the elongation of the more extended structures seen in our maps. We suggest that the compact double structures seen at high angular resolution corresponds to the inner parts of the biconical jets of ionized gas, as expected from theoretical considerations (cf. Rodríguez et al. 1990).

3.1.2. Pre-Main-Sequence Stars: Objects 3a, 8, and 9

Objects 3a, 8, and 9, located in the central part of Cep A-East region, are characterized by being unresolved and by exhibiting considerable variations in their flux densities. Further, object 3a coincides with a weak 1μ point source (Lenzen 1988), and is associated with an H_2O maser spot (Cohen et al. 1984). At the epoch of our observations, source 8 had a large negative spectral index, while source 9 exhibited a flat spectrum. Hughes (1988, 1991) has discussed possible interpretations for the radio emission from objects 8 and 9 concluding that the emission mechanism is likely to be gyrosynchrotron emission. Surveys of star forming regions at radio wavelengths show that the kind of flare activity exhibited by sources 8 and 9 is characteristic of pre-main sequence stars (André, Montmerle, & Feigelson 1987, Montmerle & André 1988). Thus, on the basis of their observed characteristics we suggest that these three objects have energy sources of their own, probably low mass pre-main-sequence stars.

3.2. Externally Excited Objects

The radio sources within this group (objects 1a, 1b, 4, 5, 6, 7a, 7b, 7c, and 7d) are characterized by being less bright than the internally excited sources, by exhibiting extended halos of diffuse emission, and by being found in chains or strings (strings 1, '456', & 7). A notable characteristic of these sources is that they are

located at the edges of dense ammonia condensations (Torrelles et al. 1985, 1986, 1993). String 1 is projected toward the northern edge of the NH_3 clump Cep A-1; string 7 is projected toward the southern border of Cep A-3; while the northern string is at the southern edge of the NH_3 clump Cep A-2.

Most of the string sources show a mixture of flat and negative spectral indices across their faces, suggesting that both thermal and nonthermal emission arises from the strings. Flat indices are usually seen toward the cores while negative indices are seen toward the envelopes, suggesting that the non-thermal emission dominates in the envelopes and/or interclump medium. This combined thermal and non-thermal emission can be expected in a shock wave moving through a magnetized medium where a fraction of the electrons will be accelerated to relativistic velocities, producing the nonthermal synchrotron emission, while most of the electrons (with a thermal distribution of velocities) will produce the thermal free-free component (Crusius-Wätzel 1990; Henricksen et al. 1991). If the density of thermal electrons is below the critical density, n_e^{th}(crit), given by

$$\left(\frac{n_e^{th}(\mathrm{crit})}{10^4\ \mathrm{cm}^{-3}}\right) = 2.1 \left(\frac{\alpha(p)}{g_{\mathrm{ff}}}\right)^{1/2} \left(\frac{T_e}{10^4\,\mathrm{K}}\right)^{1/4} \left(\frac{B}{\mathrm{mG}}\right)^{3/4} \left(\frac{E_{\mathrm{min}}}{10^{-6}\ \mathrm{ergs}}\right)^{1/2} \left(\frac{\nu}{\mathrm{GHz}}\right)^{-1/4} \left(\frac{n_{er}}{10^{-3}\ \mathrm{cm}^{-3}}\right)^{1/2} , \quad (1)$$

where n_{er} is the density of the non-thermal electrons, B is the magnetic field, T_e is the electron temperature, and E_{min} is the minimum energy of the relativistic electrons, then the synchrotron radiation will dominate the free-free radiation. The quantity g_{ff} is the Gaunt factor for free-free emission and $\alpha(p)$, where p is the energy spectral index, is the standard synchrotron radiation factor as defined by Lang (1980).

The spectral indices of the integrated emission from sources 1b, 4, 6, and 7a are between -0.3 and -0.1. They are somewhat smaller, but consistent within the errors, with those expected for optically thin thermal emission. Assuming that the emission from these sources is thermal radiation from a plasma with an electron temperature of 10^4 K, from the observed parameters (flux density and size) we derive thermal electron densities of $\sim 1 \times 10^4$ cm^{-3}, emission measures of $\sim 1 \times 10^6$ pc cm^{-6}, and number of ionizing photons required for excitation of $\sim 2 \times 10^{44}$ s^{-1}. On the other hand, the spectral indices of the integrated radio emission from the string sources 1a, 5, 7b and 7c , ≤ -0.4, are characteristic of non-thermal emission. Assuming that the radio emission from these sources is synchrotron radiation from electrons that are accelerated in the region of interaction between the wind from a central star and the ambient cloud material, from the observed parameters we derive that the strength of the magnetic field is typically $\sim$0.3 mGauss and that the density of relativistic electrons is $\sim 5 \times 10^{-4}$ cm^{-3}.

We suggest that the radio emission from the string sources arises from shock excited ionized gas at the interface between the confined winds and the molecular clumps. The non-thermal radiation is likely to be the result of the acceleration of a small fraction of the electrons in the bow shocks, formed by the interaction of the stellar wind and ambient high density clumps, by the diffusive shock acceleration mechanism. The detection of non-thermal and thermal emission from different regions of a string feature (for instance sources 7a and 7b) allows a direct test of the model proposed here. Assuming that the emission from source 7b, which exhibits a large negative spectral index, is entirely non-thermal we derive B $\sim$ 0.34 mGauss and $n_{er}E_{min} \sim 9.4 \times 10^{-10}$ ergs cm^{-3}. Replacing these values in expression (1), using $\alpha(2)$ =2.06 and g_{ff}=5.76, we find that the critical density is 5.0×10^3 cm^{-3}. The expectation then is that the density of the thermal electrons within source 7a, which exhibits a flat spectrum suggestive of thermal emission, should be higher than this critical density, which is in agreement with the derived value of 2.5×10^4cm^{-3}.

We conclude then, that both the thermal and non-thermal emission from the string sources originates from within a magnetohydrodynamic shock front resulting from the interaction of a stellar wind or outflow with dense molecular clumps (Curiel, Cantó, & Rodríguez 1987, McKee & Hollenbach 1987). A similar scenario has been proposed by Curiel et al. (1993) to explain a similar mixture of positive, flat, and negative spectral indices observed in the Serpens radio jet. In both cases, the flat and positive spectral indices are associated to the brighter knots, while the negative indices appear associated to the faint and extended emission between the clumps, and there seem to be a gradual transition between positive and negative indices (at least at the observed angular resolution). Although the origin of the radio thermal and nonthermal emission in both region is the same (the radio emission is produced by electrons accelerated and compressed in a shock wave), the origin of the emitting shock wave seems to be different, however. The knotty structure of the Serpens radio jet has been interpreted as the result of discrete ejection of material (time variable wind or "bullets") from the central source, where the radio emission is produced by the shock wave preceding the condensations moving through the ambient medium. In the Cep A-East case, we have not observed proper motions in any of the knots (upper limit of 0.″02 per year), suggesting that the radio emission is either produced by condensations moving at steep angles with respect to the plane of the sky (almost along the line of sight) or that the shock waves are quasi static with respect to the ambient medium.

4. DRIVING SOURCES OF ACTIVITY

We argued above that the radio emission from the string sources arises from shock excited gas at the edge of molecular structures powered by a stellar wind from an external source, and therefore that the string sources do not contain energy sources of their own. The question arises as to which is (or are) the powering source of the chain features. We suggest that they are powered by objects 2 and 3d, whose morphologies and dependences of flux density and angular size with frequency imply that they correspond to collimated thermal jets. We propose that the excitation of the radio strings 1 and '456', which are roughly aligned along the jet axis of source 2 (P.A. of 44°) is produced by shock waves driven by the confined stellar wind that arises from this object. In addition, we propose that the excitation of string 7 might be produced as the confined wind from source 3d –whose major axis, at a P.A. of 107°, appears elongated in the direction of the string 7– impinges on the edge of the Cep A-3 NH_3 cloud.

Observations with 15″ angular resolution have shown that the outflowing CO molecular gas toward Cep A-East is quadrupolar, consisting of two *blueshifted-redshifted* pair of lobes oriented in directions with P.A. of ∼30° and ∼100° (Bally & Lane 1991). Gómez et al. (1995) observed the HCO^+ line emission from this region, with ∼3″ resolution, and found a high density, high velocity, bipolar flow oriented roughly at a P.A of 45°. It is interesting to note that the direction of the elongation of source 3d, as well as the orientation of the alignment of its ultracompact components, have roughly the same position angle than that of the *east-west* pair of lobes of the large scale quadrupolar molecular flow. Further, the direction of the major axis of jet 2 is similar to the position angle of the pair of lobes of the high density flow. Thus, it is possible that the large scale quadrupolar molecular structure might be produced by the winds from these two outflow sources, rather than being produced by the structure of the environment as suggested by Torrelles et al. (1993).

In summary, we suggest that most of the complex activity (molecular outflows and radio strings) observed within the Cep A-East region is powered by objects 2 and 3d. The confined stellar wind from object 2 excites the radio strings 1 & '456' and drives the NE-SW high density bipolar outflow. The collimated thermal jet from object 3d excites the radio string 7 and drives the low velocity E-W bipolar outflow. The question whether there are other sources driving some of the activity seen in the Cep A-East region is still open, however. For instance, a potential candidate for the energy source of the ellipse of HH emission seen towards Cep A, possible driven by a poorly collimated wind (Corcoran et al. 1993), is the variable radio source 9 which is located near the apex of the ellipsoidal feature.

The work presented in this contribution has been done in collaboration with my colleagues L. F. Rodríguez, S. Curiel, and J. M. Torrelles. I gratefully acknowledge the support of a Guggenheim Fellowship and the warm hospitality received at the Instituto de Astronomía, UNAM.

REFERENCES

André, P., Montmerle, T., & Feigelson, E. D. 1987, AJ, 93, 1182
Bally, J., & Lane, A. P. 1991, ASP Conf. Ser., 14, 273
Blitz, L., & Lada, C. J. 1979, ApJ, 227, 152
Cohen, R. J., Rowland, P. R., & Blair, M. M. 1984, MNRAS, 210, 425
Corcoran, D., Ray, T. P., & Mundt, R. 1993, A&A, 279, 206
Crusius-Wätzel, A. R. 1990, ApJ, 361, L49
Curiel, S., Cantó, J., & Rodríguez , L. F. 1987, RevMexAA, 14, 595
Curiel, S., Rodríguez , L.F., Moran, J. M., & Cantó, J. 1993, ApJ, 415, 191
Evans, N. J., Becklin, E. E., Beichman, C., Gatley, I., Hildebrand, R. H., Keene, J., Slovak, M. H., Werner, M. W., & Whitcomb, S. E. 1981, ApJ, 244, 115
Garay, G., Ramírez, S., Rodríguez , L.F., Curiel, S, & Torrelles, J. M. 1995, ApJ, submitted
Hartigan, P., & Lada, C. J. 1985, ApJS, 59, 383
Hartigan, P., Lada, C. J., Stocke, J., & Tapia, S. 1986, AJ, 92, 1155
Hayashi, S. S., Hasegawa, T., & Kaifu, N. 1988, ApJ, 332, 354
Henriksen, R. N., Ptuskin, V. S., & Mirabel, I. F. 1991, A&A, 248, 221
Hughes , V. A. 1985, ApJ, 298, 830
Hughes , V. A. 1988, ApJ, 333, 788
Hughes , V. A. 1991, ApJ, 383, 280
Hughes , V. A., & Wouterloot, J. G. A. 1982, A&A, 106, 171
Hughes , V. A., & Wouterloot, J. G. A. 1984, ApJ, 276, 204

Lada, C. J., Blitz, L., Reid, M. J., & Moran, J. M. 1981, ApJ, 243, 769
Lang, K. R. 1980, in Astrophysical Formulae (Springer, Heidelberg)
Lenzen, R. 1988, A&A, 190, 269
Martí, J., Rodríguez , L. F., & Reipurth, B. 1993, ApJ, 416, 208
McKee, C. F., & Hollenbach, D. J. 1987, ApJ, 322, 275
Montmerle, T., & André, P. 1988, in Formation and Evolution of Low Mass Stars, ed. A. K. Dupree & M. T. V. T. Lago, 225
Raga, A. C., Cantó, J., Calvet, N., Rodríguez , L. F. & Torrelles, J. M. 1993, A&A, 276, 539
Reynolds, S. P. 1986, ApJ, 304, 713
Rodríguez , L. F., Carral, P., Ho, P. T. P, & Moran, J. M. 1982, ApJ, 260, 635
Rodríguez , L. F., & Cantó, J. 1983, RevMexAA, 8, 163
Rodríguez , L. F., Garay, G., Curiel, S., Ramírez , S., Torrelles, J. M., Gómez, Y., & Velázquez, A. 1994, ApJ, 430, L65
Gómez, J., et al. 1995, in preparation
Rodríguez , L. F., Ho, P. T. P., & Moran, J. M. 1980, ApJ, 240, L149
Rodríguez , L. F., Ho, P. T. P., Torrelles, J. M., Curiel, S., & Cantó, J. 1990, ApJ, 352, 645
Rodríguez , L. F., Moran, J. M., Ho, P. T. P., & Gottlieb, E. W. 1980, ApJ, 235, 845
Sargent, A.I . 1977, ApJ, 218, 736
Torrelles, J. M., Ho, P. T. P., Rodríguez , L.F., & Cantó, J. 1985, ApJ, 288, 595
Torrelles, J. M., Ho, P. T. P., Rodríguez , L. F., & Cantó, J. 1986, ApJ, 305, 721
Torrelles, J. M., Verdes-Montenegro, L., Ho, P. T. P., Rodríguez , L. F., & Cantó, J. 1993, ApJ, 410, 202

object and may actually have a symbiotic relationship. Although a generally accepted model for this situation with simultaneous infall and outflow has yet to be produced, current notions are consistent with young stars having a protoplanetary disk in Keplerian rotation with dimensions of order 100 AU. Part of the rotational energy of this disk, most probably via a magnetohydrodynamic mechanism, is used to power the collimated jets that in its turn give rise to the bipolar outflows and Herbig-Haro objects. In return, the jet may carry away angular momentum, alleviating the well-known problem of excess angular momentum in the system.

Despite major observational advances obtained from low angular resolution studies, it appears clear that a deep understanding of disks and jets in young stars will only be achieved with subarcsecond observations of these objects (equivalent to tens of AUs at the distance of the closest regions of low-mass star formation), since it is at these scales that the protoplanetary disks are expected to become angularly resolved and over which jet acceleration and collimation may be taking place.

In this paper, I review some recent results obtained with subarcsecond angular resolution continuum observations toward young stars at centimeter and millimeter wavelengths. As discussed by Gómez & D'Alessio (1995) in these Proceedings, eventually these subarcsecond observations will have to include spectroscopic capability for a more complete description, but these observations are still in the future. A previous review on disks and outflows is given by Rodríguez (1994). A review of thermal jets from a more general perspective is presented by Anglada (1995) in these Proceedings. Centimeter radio continuum emission is detected not only from the thermal jets very close to the exciting source, but also from the more separated Herbig-Haro objects, and Curiel (1995) has discussed this topic in detail in these Proceedings.

A major problem with the subarcsecond observations of thermal processes is the modest flux density contained in the very small synthesized beam. When observing a source with brightness temperature T_B, at a frequency ν, with a circular beam with angular diameter θ_B, the flux density inside the beam will be given by

$$\left[\frac{S_\nu}{mJy}\right] = 0.40 \left[\frac{\nu}{8.4\ GHz}\right]^2 \left[\frac{T_B}{10^3\ K}\right] \left[\frac{\theta_B}{0.1\ arc\ sec}\right]^2 \quad (1)$$

This equation implies that very sensitive instruments are required for the study of thermal processes with high angular resolution. For free-free emission, it is expected that $T_B \leq 10^4\ K$, while for thermal emission from dust one usually will have $T_B \leq 10^2\ K$. Most of the observations discussed here were obtained with the Very Large Array (VLA) of the National Radio Astronomy Observatory that with its large collecting area is the most sensitive radio telescope in the 0.1 arc sec scale of angular resolution.

2. SUBARCSECOND OBSERVATIONS OF THERMAL JETS AT CENTIMETER WAVELENGTHS

What is a thermal jet? We can define it as a small ($\leq 1''$) continuum source with elongated morphology and thermal (that is, flat or rising with frequency) spectrum. The thermal jet is expected to be two-sided (bipolar), located at the center of an outflow, and with its major axis well-aligned with the outflow axis, as defined by the presence of Herbig-Haro objects and bipolar molecular outflows on much larger physical scales. In general thermal jets are found in association with low luminosity ($\leq 100\ L_\odot$) sources. Perhaps the best example of this prototypical thermal jet is VLA 1 in the HH1-2 region (Rodríguez et al. 1990). However, departures from these characteristics have been found and in what follows we discuss several sources that have shown to us that the phenomenon is quite diverse.

2.1. The One-Sided Thermal Jet in HH 111

Some of the jets, as observed in the radio, infrared, or optical wavelengths, can show remarkable symmetry in their inner morphology as well as in the sequence of knots that can be detected on both sides of the jet. An example of a symmetric jet on the arc sec scale is HH 80-81 (discussed below). On larger scales (tens of arc sec) jets studied by means of the v=1-0 S(1) line of molecular hydrogen (HH211; McCaughrean, Rayner, & Zinnecker 1994) or millimeter molecular transitions (L1448; Bachiller et al. 1990) can also be quite symmetric.

However, not all jets are symmetric. Using long-slit spectroscopy of forbidden lines, Hirth et al. (1994) have proposed that jets from T Tauri stars can show large differences in the velocities of the redshifted and blueshifted parts of the jet. A more direct evidence for asymmetries in jets is provided by the 3.5 cm VLA map of the jet in HH 111 presented by Rodríguez & Reipurth (1994). As can be seen in Figure 1, on the subarcsecond scale this jet appears to be one-sided.